

Ab initio calculations of elastic constants of plagioclase feldspars

PAMELA KAERCHER^{1,*}, BURKHARD MILITZER^{1,2} AND HANS-RUDOLF WENK¹

¹Department of Earth and Planetary Science, University of California, Berkeley, California 94720, U.S.A.

²Department of Astronomy, University of California, Berkeley, California 94720, U.S.A.

ABSTRACT

Plagioclase feldspars comprise a large portion of the Earth's crust and are very anisotropic, making accurate knowledge of their elastic properties important for understanding the crust's anisotropic seismic signature. However, except for albite, existing elastic constants for plagioclase feldspars are derived from measurements that cannot resolve the triclinic symmetry. We calculate elastic constants for plagioclase end-members albite $\text{NaAlSi}_3\text{O}_8$ and anorthite $\text{CaAl}_2\text{Si}_2\text{O}_8$ and intermediate andesine/labradorite $\text{NaCaAl}_3\text{Si}_5\text{O}_{16}$ using density functional theory to compare with and improve existing elastic constants and to study trends in elasticity with changing composition. We obtain elastic constants similar to measured elastic constants and find that anisotropy decreases with anorthite content.

Keywords: Plagioclase feldspars, elastic constants, ab initio calculations, seismic anisotropy

INTRODUCTION

Plagioclase feldspars are one of the most important rock-forming minerals, comprising roughly 40% of the Earth's crust. Thus their elastic properties are essential for interpreting seismic data to determine the structure and deformation history of the Earth's crust, especially the seismically anisotropic lower crust. Anisotropy in an aggregate depends on the preferred orientation of crystals and the single-crystal elastic constants. While many studies have quantified the effect of crystallographic preferred orientation on seismic anisotropy in natural plagioclase-rich samples (e.g., Liebermann and Ringwood 1976; Wenk et al. 1986; Ji and Mainprice 1988; Siegesmund et al. 1989; Siegesmund and Kruhl 1991; Seront et al. 1993; Xie et al. 2003; Feinberg et al. 2006; Barreiro et al. 2007) and found *p*-wave anisotropy to be as high as 15%, few data of single-crystal elastic constants of plagioclase exist.

Alexandrov and Ryzhova (1962) calculated elastic constants from acoustic wave velocities through plagioclase comprised of 58% anorthite and 42% albite (denoted as An58), Ryzhova (1964) made similar measurements for An9, An24, An29, An53, and An56, and more recently, Brown et al. (2006) for An0. The elastic constants published by Alexandrov and Ryzhova (1962) and Ryzhova (1964) are widely cited in literature and handbooks (e.g., Simmons and Wang 1971; Every and McCurdy 1992; Bass 1995; Hacker and Abers 2004), yet, although carefully measured, they could not resolve the triclinic symmetry. Using the ultrasonic pulse method, Alexandrov and Ryzhova (1962) and Ryzhova (1964) were able to measure only three polarizations for six directions, which is not enough to constrain elastic constants for even monoclinic symmetry. Because of twinning, monoclinic crystal symmetry was assumed in the measurements of Ryzhova (1964), and only 13 elastic constants were determined rather than 21. In addition microcracks were not characterized

and taken into account.

Further uncertainty is introduced when elastic constants are calculated from measured velocities using the Kelvin-Christoffel equations (Musgrave 1970). Kelvin-Christoffel equations use phase velocities, whereas ultrasonic measurements involve group and phase velocities, and the difference can be large for highly anisotropic crystals with low symmetry like plagioclase. Alexandrov et al. (1974) recalculated C_{ij} s from the measurements of Ryzhova (1964) but without clear improvements. In fact, C_{12} , C_{23} , and C_{25} for An9 of Alexandrov et al. (1974) greatly deviate (20, 34, and 195%, respectively) from values of Ryzhova (1964) and are also inconsistent for C_{12} , C_{23} , and C_{25} calculated by Alexandrov et al. (1974) for the other compositions (An24, An29, An53, and An56). Seront et al. (1993) measured acoustic velocities through an anorthosite rock composed of 90% plagioclase with composition An68 and 10% olivine and adjusted the elastic constants of Ryzhova (1964) by an average of 10%, and the recalculations of Alexandrov et al. (1974) by more, to account for their measured velocities. Because of the larger errors found in the recalculations of Alexandrov et al. (1974), we will compare results with the original calculations of Ryzhova (1964) in this paper.

The measurements of Seront (1993) demonstrated that a difference of 10% in elastic constants has a notable effect on acoustic velocities. Besides disagreement between the C_{ij} for albite of Ryzhova (1964) and Alexandrov et al. (1974), newer measurements also disagree. Brown et al. (2006) measured 162 velocities in 125 propagation directions through an untwinned single crystal of An0 using impulsively stimulated light scattering [ISLS, method described in Abramson et al. (1999)] and retrieved all 21 elastic constants needed for triclinic symmetry. Brown's values vary by as much as 44 GPa for some C_{ij} compared with earlier measurements (Ryzhova 1964) signifying large errors in one or both sets of data.

No first-principles calculations of plagioclase feldspar elastic constants yet exist to compare with these experimental

* E-mail: p.kaercher@berkeley.edu

results. We have performed ab initio calculations using density functional theory (DFT) to calculate elastic constants for albite $\text{NaAlSi}_3\text{O}_8$ (An0), andesine/laboradorite $\text{NaCaAl}_3\text{Si}_5\text{O}_{16}$ (An50), and anorthite $\text{CaAl}_2\text{Si}_2\text{O}_8$ (An100) to assess and improve upon the precision of existing elastic constants. We provide the first full set of elastic constants for An50 and the first set of non-extrapolated elastic constants for An100. With these calculations we briefly explore the separate effects of composition and structure on elastic constants in the plagioclase mineral family.

STRUCTURES

The feldspar framework contains TO_4 tetrahedra with Al and Si cations occupying tetrahedral sites (T-sites, nomenclature from Ribbe 1983). Four T-sites exist in plagioclase feldspars that cannot be related by symmetry: T_{1o} , T_{2o} , T_{1m} , T_{2m} . These four T-sites are linked in a ring by their neighboring oxygen atoms [O_b and O_d , nomenclature from Megaw (1956)] and stack parallel to the b -axis. The two bonding oxygen atoms, O_a and O_c , alternate in the $[010]$ direction, linking the layers of rings together. The O_a atoms bridge the tetrahedra to the larger cations (M-sites) while the O_c atoms do not (Megaw et al. 1962). A three-dimensional unit cell of albite (An0) is illustrated in Figure 1.

An important characteristic of feldspars is the distribution of Al atoms in T-sites. In An0, only one tetrahedron in each ring contains an Al atom, and at room temperature (i.e., in low albite), Al occupies only T_{1o} sites. Ordering of Al into the T_{1o} sites in An0 is due to π -bonding effects which render Si-O-Si angles larger than Al-O-Si angles; because the average structure of An0 has $T_{2m}\text{-O}_{\text{bm}}\text{-T}_{1m}$ and $T_{1m}\text{-O}_{\text{am}}\text{-T}_{2o}$ angles both larger than 150° , Si atoms preferentially fill the T_{2m} , T_{1m} , and T_{2o} sites, leaving the Al to fill the T_{1o} sites (Stewart and Ribbe 1969). This is not the case in albite that has been heated (Tuttle and Bowen 1950; Laves and Chassignon 1950) (i.e., high albite), where entropy favors Al partial occupation of all four T-site types. In An100

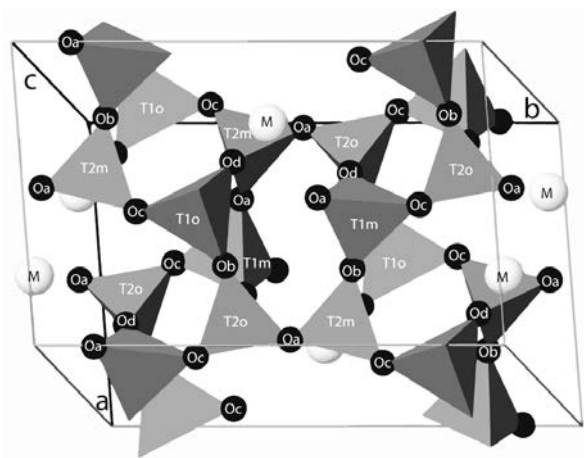


FIGURE 1. Three-dimensional illustration of an albite (An0) unit cell; andesine (An50) and anorthite (An100) unit cells are similar but twice the length in c . T-sites (gray) are most often occupied by Al or Si, and M-sites (white) are mostly occupied by Na or Ca in plagioclase feldspars. Oxygen sites are black. The unit cell is outlined with thin lines, and axes a , b , and c are in thick black.

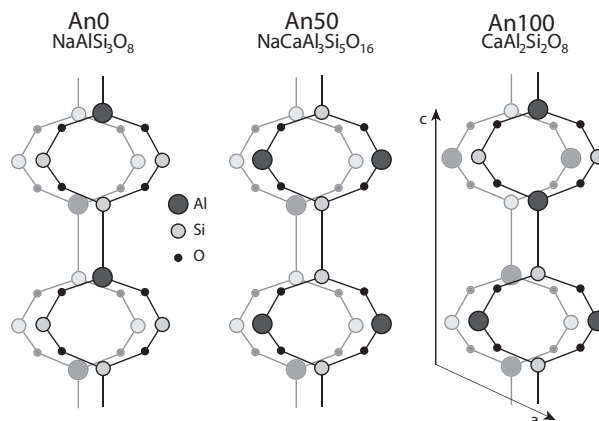


FIGURE 2. Simple schematic showing Al positions in tetrahedral rings as viewed down the b -axis in An0 Model 1, An50 Model 1, and An100. Larger dark gray circles represent tetrahedra occupied by Al, smaller light gray circles represent tetrahedra occupied by Si, and small black circles represent O atoms.

two of the four tetrahedral sites contain Al. Here Al occupies all four T-site types due to alternation of Al and Si to satisfy the Al-avoidance rule (Loewenstein 1954; Wenk and Kroll 1984; Smith and Brown 1988, p. 52–53). A simple schematic of the tetrahedral rings as seen looking down the b -axis for An0, An50, and An100 is shown in Figure 2.

The effect of Al distribution within T-sites has been widely studied (e.g., Ferguson et al. 1958; Ribbe et al. 1969; Prewitt et al. 1976; Winter et al. 1979; Carpenter et al. 1985, 1990; Kunz and Armbruster 1990; Sochalski-Kolbus et al. 2010), and has been found to play an important role in the topology of the tetrahedral framework. Because Al atoms are larger than Si atoms, the Al-O bonds are longer than Si-O bonds. The difference in Al-O and Si-O bond lengths is accommodated by the T-O-T bond angles (the angles between tetrahedra) (e.g., Megaw et al. 1962; Ribbe 1983; Smith and Brown 1988, p. 66–67; Wenk and Kroll 1984), thus causing tetrahedra to tilt to maximize the shortest O-O distances (Tribaudino and Angel 2012). The tetrahedral tilt that accompanies increasing An-content decreases elastic anisotropy, which we later discuss.

Distribution of Al in plagioclase also affects unit-cell symmetry. In low An0, where Al occupies only T_{1o} sites, two rings are equivalent by translation along the c -axis, and the unit cell has symmetry $C\bar{1}$. In intermediate plagioclase, such as An50, the distribution of Al and Si is reversed from one tetrahedral ring to the next (Fig. 2), making the rings no longer equivalent by translation along the c -axis. Thus, the unit cell is doubled in the c direction, and the symmetry is lowered to $\bar{1}1$. Symmetry is lowered further to $P\bar{1}$ for compositions near the An100 end-member, because atomic positions in tetrahedral rings centered at $c \sim 1/4$ and $c \sim 3/4$ are no longer equivalent (e.g., Kempster et al. 1962; Wenk and Kroll 1984). Cell parameters also change systematically but not linearly as content progresses from An0 to An100 (Smith and Brown 1998, p. 165–168). Parameter a increases by $\sim 0.5\%$, and b increases by $\sim 0.6\%$ with An-content until An80 where it remains mostly constant, while parameter c

decreases by ~0.7% with An-content. Angles α and β decrease by ~1° with An-content. The angle γ increases significantly (>3° total) with An content, but not steadily—not much change happens from ~An33–An67, perhaps due to a pronounced onset of Al-disorder (e.g., Bambauer et al. 1967; Kroll and Müller 1980; Kroll 1983; Benna et al. 1985).

The effects of An content, Al disorder, and large cation placement on elasticity in plagioclase feldspars can be systematically studied more readily with calculations. We briefly look at the influence of each by calculating elastic constants for three An0 structures, three An50 structures, and one An100 structure.

Model An0

The An0 structures are based on the structure determined by Harlow and Brown (1980) by neutron diffraction. Their sample was a natural low albite from Amelia County, Virginia, with Al almost exclusively occupying T₁₀-sites according to measured T-O bond lengths. Cell parameters are $a = 8.142(2)$ Å, $b = 12.785(2)$ Å, $c = 7.159(2)$ Å, $\alpha = 94.19(2)^\circ$, $\beta = 116.61(2)^\circ$, and $\gamma = 87.68(2)^\circ$. Additional information about the sample (no. 6306) is given in Waldbaum and Robie (1971).

Three An0 models were defined. An ideal NaAlSi₃O₈ composition was assumed. Atomic positions and cell parameters were relaxed (relaxation described in Methods section) from values given in Harlow and Brown (1980), and changed slightly. Model 1 is an ordered albite structure in which T₁₀ were filled with only Al, and all other T-site types, with Si. The placement of Al and Si among tetrahedra in Model 1 is shown in Figure 2. To assess the effect of Al disorder, we constructed a second unit cell, Model 2, identical to that of Model 1 but with Al partially occupying all T-site types. This structure has the lowest Coulomb energy of all such fully disordered Al-configurations but is still 15 eV (~2200 K kinetic temperature) higher than Model 1. This large energy difference arises from our use of only one unit cell in calculations, which requires the same four T-sites to be occupied by Al in every unit cell. More realistically, the Al would occupy all four T-site types, but not always the same T-sites in every cell (there are four of each type per cell), and some such configurations will have a lower energy. For Model 3, the unit cell was doubled in size along the *c*-axis to allow more variability of Al placement, and the lowest energy, fully disordered configuration was chosen. The energy difference is 14.8 eV higher than for Model 1. To significantly reduce the energy in the disordered structure, a super cell must be used, which would increase computational time by many orders of magnitude, making methods used here not ideal for a careful study of Al-disorder. Nonetheless, as discussed below, our results for disordered albite using one or two unit cells are still meaningful.

Model An50

The An50 structures were modified from the An48 sample of FitzGerald et al. (1986), a volcanic plagioclase megacryst from basalt flows from the Hogarth Ranges, Australia. Cell parameters $a = 8.179(1)$ Å, $b = 12.880(1)$ Å, $c = 14.224(1)$ Å, $\alpha = 93.44(1)^\circ$, $\beta = 116.21(1)^\circ$, and $\gamma = 90.23(1)^\circ$.

The composition was changed to NaCaAl₃Si₅O₁₆, and atomic positions and cell parameters were relaxed for each of the three An50 models. Because cation placement can affect elastic

constants, we calculated Coulomb energies for all possible arrangements of Al within the tetrahedral sites. Model 1 is the unit cell with the Al arrangement having the lowest energy (Fig. 2). A second unit cell with a different Al arrangement having 4 eV (~600 K kinetic temperature) higher energy than Model 1 was chosen to study the effect of Al placement on elastic constants. In a third structure, Model 3, two Na were swapped with two Ca to study the effect of large cation placement on elastic constants.

Model An100

The An100 structure was based on that of the sample of pure anorthite from Val Paseda, Tyrol, Austria, of Wainwright and Starkey (1971). Cell parameters are $a = 8.173(1)$ Å, $b = 12.869(1)$ Å, $c = 14.165(1)$ Å, $\alpha = 93.113(6)^\circ$, $\beta = 115.913(6)^\circ$, and $\gamma = 91.261(6)^\circ$. Atomic positions and cell parameters were relaxed, but the chemistry was not altered. Ca positions were idealized, rendering a unit cell with higher symmetry, $\bar{1}$, rather than $P\bar{1}$, which is more typical for An100 where Ca atom sites are split (Wenk and Kroll 1984). Al occupies half of the T-sites and was distributed evenly into all T-site types, alternating with Si for charge balance (see Fig. 2).

METHOD

We calculated the elastic constants of An0, An50, and An100 with density functional theory (DFT) (Hohenberg and Kohn 1964; Kohn and Sham 1965) using the Vienna Ab initio Simulation Package (VASP) (Kresse and Hafner 1993; Kresse and Furthmüller 1996). Wave functions of valence electrons were expanded by a plane wave basis set with an energy cut off of 582 eV, and sampling points in the Brillouin zone were created with a Monkhorst-Pack grid of 4×2×2 (Monkhorst and Pack 1976). We used the finite strain approach (e.g., Karki et al. 1997; Militzer et al. 2011) and calculated elastic constants (C_{ijkl}) with Hooke's Law $\sigma_{ij} = \epsilon_{kl} C_{ijkl}$, where σ_{ij} denotes directional stress, and ϵ_{kl} directional strain.

DFT calculations were done using the local density approximation (LDA) (e.g., Ceperley and Alder 1980) while holding the volume constant at the experimentally determined cell volume. LDA is a functional that approximates the exchange-correlation term in the Hamiltonian equation. It depends only on the density at the point where the functional is being evaluated whereas another commonly used approximation, the generalized gradient approximation (GGA) (Perdew et al. 1996), depends on density and energy gradient at the point being evaluated. Both LDA and GGA produce errors: LDA shortens and tightens bonds, overestimating density, and GGA underestimates the density. To reduce density errors, unit cells were first relaxed at constant volume to preserve the density while optimizing electronic and ionic positions until all forces were <10³ eV/Å. Similar methods of using experimental volumes when calculating LDA forces have been used by White et al. (2009) for kaolinite. Note that the densities for An0 and An50 used in calculations do not exactly equal experimentally determined densities, because we slightly modified their compositions to be stoichiometric. Elastic constants for An0 were calculated using both LDA and GGA and are compared with experimental results in Table 1 and Figure 3. Because of better agreement with experimental results for nearly all elastic constants, which we later discuss, we chose LDA as the exchange correlation functional for all other calculations.

After relaxation, the lattice vectors of the unit cells ($\mathbf{a}, \mathbf{b}, \mathbf{c}$) $\equiv \mathbf{A}$ were strained to new lattice vectors ($\mathbf{a}', \mathbf{b}', \mathbf{c}'$) $\equiv \mathbf{A}'$ by $\mathbf{A}' = (\mathbf{I} + \epsilon) \mathbf{A}$, where \mathbf{I} is the identity matrix, and ϵ is the strain matrix. In Voigt notation, the three diagonal ($i = 1, 2, 3$) and three off-diagonal ($i = 4, 5, 6$) strain tensors are defined similar to

$$\epsilon_i = \begin{pmatrix} \delta & 0 & 0 \\ 0 & 0 & 0 \\ 0 & 0 & 0 \end{pmatrix} \text{ and } \epsilon_4 = \begin{pmatrix} 0 & 0 & 0 \\ 0 & 0 & \delta/2 \\ 0 & \delta/2 & 0 \end{pmatrix}$$

For each tensor, a positive and a negative strain of magnitude $\delta = \pm 0.005$ was applied, the atomic positions were relaxed, and stresses were calculated. The elastic constants were determined from the stress-strain relationship. The resulting C_{ij} matrix was symmetrized in the final step of the calculation.

We estimate total errors in elastic constants to be less than ± 2 GPa based on

TABLE 1. Cell parameters and stiffness coefficients C_{ij} (where i and j are indices in Voigt notation) calculated for An0, An50, and An100; experimentally (exp.) derived elastic constants for similar plagioclase compositions from Brown et al. (2006) (B), Ryzhova (1964) (R), and Alexandrov and Ryzhova (1962) (A&R) are also shown

Struct. Method	An0 1 LDA	An0 1 GGA	An0 2 LDA	An0 3 LDA	An0 B exp.	An9 R exp.	An50 1 LDA	An50 2 LDA	An50 3 LDA	An53 R exp.	An58 A&R exp.	An100 LDA
a (Å)	8.153	8.091	8.182	8.152	8.13662	–	8.188	8.198	8.192	–	–	8.163
b (Å)	12.776	12.842	12.856	12.853	12.7857	–	12.881	12.869	12.880	–	–	12.894
c (Å)	7.181	7.197	7.101	14.207	7.1582	–	14.235	14.175	14.226	–	–	14.176
α (°)	94.65	94.24	94.57	93.96	94.253	–	94.33	95.11	94.79	–	–	93.753
β (°)	116.96	116.99	116.70	116.43	116.605	–	116.36	115.74	116.27	–	–	116.025
γ (°)	87.62	87.76	90.35	90.13	87.756	–	88.91	89.26	88.80	–	–	90.872
ρ (g/cm ³)	2.62	2.62	2.62	2.62	2.62	2.61	2.68	2.68	2.68	2.68	2.68	2.77
C_{11}	63.6	82.3	72.2	64.6	69.9	66.8	99.2	95.2	100.7	86.0	101.1	125.3
C_{22}	159.2	173.5	149.6	148.3	181.1	137.0	169.4	158.5	167.6	162.5	158.2	178.3
C_{33}	165.7	179.2	153.8	144	180.7	143.6	165.2	162.6	163.2	151.3	148.4	167.0
C_{44}	28.3	28.7	22.15	23.25	25.6	21.6	25.1	26.7	23.0	24.7	22.2	23.7
C_{55}	22.8	28.5	23.2	24	26.8	26.7	28.5	29.0	29.1	33.2	34.8	35.6
C_{66}	34.2	32.4	39.65	36.4	33.5	27.3	37.5	39.7	38.3	32.3	36.3	41.3
C_{12}	31.8	44.5	34.65	27.25	34.7	27.3	50.3	50.3	50.1	43.9	60.6	58.1
C_{13}	26.8	39.7	30.5	24.85	30.0	34.0	38.5	37.7	38.3	44.5	49.3	52.8
C_{15}	-3.7	-0.8	2.3	1.18	-2.3	0.0	-0.2	0.2	-0.1	-1.6	0.7	-0.8
C_{23}	14.9	23.7	9.75	5.45	6.3	42.3	22.0	21.6	22.4	44.1	27.1	32.7
C_{25}	-6.6	-4.2	-3.55	-3.9	-7.5	-7.6	-2.1	-1.3	-1.4	-8.5	-10.1	-0.1
C_{35}	7.0	7.3	9.27	10.97	8.0	4.5	6.7	8.7	6.0	4.1	11.6	5.5
C_{46}	-5.0	-5.0	-3.42	-4.55	-7.6	-6.2	-0.3	0.5	-3.8	-7.9	-6.5	7.2
C_{14}	5.1	3.8	7.1	4	4.7		9.6	7.0	10.2			9.2
C_{16}	-0.6	-0.5	-5.1	-2.85	-0.9		-1.1	-4.7	-0.6			-8.4
C_{24}	-10.4	-10.6	-11.55	-13.53	-13.2		-4.8	-7.7	-3.1			0.3
C_{26}	-5.0	-4.8	-9.35	-6.5	-6.9		-2.5	-2.8	-4.9			-11.6
C_{34}	3.9	4.5	-4.25	-2.87	0.5		8.7	6.4	6.5			13.8
C_{36}	-8.7	-8.7	-14.72	-11.07	-8.3		-9.3	-10.5	-8.4			-9.3
C_{45}	-1.4	-1.7	-0.97	-0.7	-0.7		-0.5	-0.8	-0.5			0.1
C_{56}	0.1	0.4	-0.45	-0.5	-0.1		0.0	-1.0	-0.3			0.2
K_v	59.5	72.3	58.4	52.4	63.7	61.6	72.8	70.6	72.5	73.9	75.7	84.2
K_r	50.3	65.5	52.3	46.5	55.2	53.2	53.2	66.9	68.6	68.5	74.6	76.3
K_h	54.9	68.9	55.3	49.5	59.5	57.4	63.0	68.8	70.6	71.2	75.2	80.3
G_v	38.0	39.7	37.0	36.7	41.2	31.4	39.7	39.5	39.5	35.9	36.7	41.9
G_r	29.5	32.3	27.5	28.2	29.8	26.9	26.9	33.5	32.4	31.2	31.0	34.6
G_h	33.8	36.0	32.3	32.4	35.5	29.1	33.3	36.5	35.9	33.5	33.8	38.3

Notes: Bulk (K) and shear (G) moduli for each set of elastic constants using Voigt (v), Reuss (r), and Hill (h) averaging are shown in the last two columns. All moduli are in GPa and are consistent with the conventional orientation $\mathbf{Z}||\mathbf{c}$, $\mathbf{Y}||\mathbf{a}$, $\mathbf{X}||\mathbf{Y}\times\mathbf{Z}$.

comparison of differences between C_{ij} and C_{ji} values, planewave basis energy cut-offs, k-space sampling, and observations of the effect of different values of δ on elastic constants. Each C_{ij} and C_{ji} were calculated separately and were found to differ by less than 0.5 GPa for all sets of elastic constants. To quantify errors associated with the planewave basis energy cut off (582 eV) and k-space sampling ($4\times 2\times 2$), we calculated An0 elastic constants with the cut off energy set to 782 and 982 eV and k-space sampling set to $2\times 2\times 2$ and $4\times 2\times 4$; all results differ by <0.5 GPa for all elastic constants. To ensure that we are in the linear strain regime, we also calculated An0 elastic constants with $\delta = 0.0025$ and $\delta = 0.0075$ and obtained elastic constants which differ by <1 GPa. All ab initio calculations were done at 0 K. However, Ab initio calculations performed at room temperature and at 0 K for the same structure return elastic constants which are not significantly different from each other (Militzer et al. 2011).

RESULTS AND DISCUSSION

Here we present and compare our elastic constants to previously published elastic constants and compression experiments on plagioclase. We also discuss differences among our various models for An0, An50, and An100. All crystal structures were oriented according to the conventional standard orientation with $\mathbf{Z}||\mathbf{c}$, $\mathbf{Y}||\mathbf{a}$, and $\mathbf{X}||\mathbf{Y}\times\mathbf{Z}$ where $(\mathbf{a}, \mathbf{b}, \mathbf{c})$ are the unit-cell axes, and $(\mathbf{X}, \mathbf{Y}, \mathbf{Z})$ are the reference frame axes in a right-handed orthogonal coordinate system (e.g., Standards on Piezoelectric Crystals 1949; Nye 1984). We have rotated Ryzhova (1964), Alexandrov and Ryzhova (1962), and Brown et al. (2006) into the same conventional orientation and show all elastic constants

(Table 1), graphs (Figs. 3–5), and velocity maps (Fig. 6) in this orientation. Because Ryzhova (1964) did not provide cell parameters, the cell angles of Brown et al. (2006), $\alpha = 94.25^\circ$, $\beta = 116.61^\circ$, and $\gamma = 87.76^\circ$, were assumed when rotating the An9 elastic constants of Ryzhova (1964), and the cell angles of FitzGerald et al. (1986), $\alpha = 93.44^\circ$, $\beta = 116.21^\circ$, and $\gamma = 90.23^\circ$, were assumed when rotating the An53 of Ryzhova (1964). We also rotated the elastic constants of Ryzhova (1964) into the orientation of Brown et al. (2006) and obtained $C_{44} = 21.0$, $C_{46} = -6.3$, and $C_{66} = 27.3$ GPa, while Brown et al. (2006) published $C_{44} = 22.5$, $C_{46} = -7.4$, and $C_{66} = 25.8$ GPa.

Calculated cell parameters are presented in Table 1. Nearly all cell parameters changed by 1% or less during relaxation, with the exception of γ , which increased by $\sim 3^\circ$ for An0 Model 2—consistent with experimental observations of larger γ in disordered albite compared to ordered albite (Benusa et al. 2005; Curetti et al. 2011)—and decreased by 1.5% for An50 Model 1. Our calculated cell parameters agree well with experimental parameters because we adopted the experimental density. However, differences do exist, likely due to the idealized unit cell that we defined, which lacks dislocations, vacancies, and atomic substitutions likely present in measured samples. Still the calculated cell parameters follow the same trend in cell parameters with An content (e.g., $\alpha_{\text{An0}} > \alpha_{\text{An50}} > \alpha_{\text{An100}}$) discussed earlier.

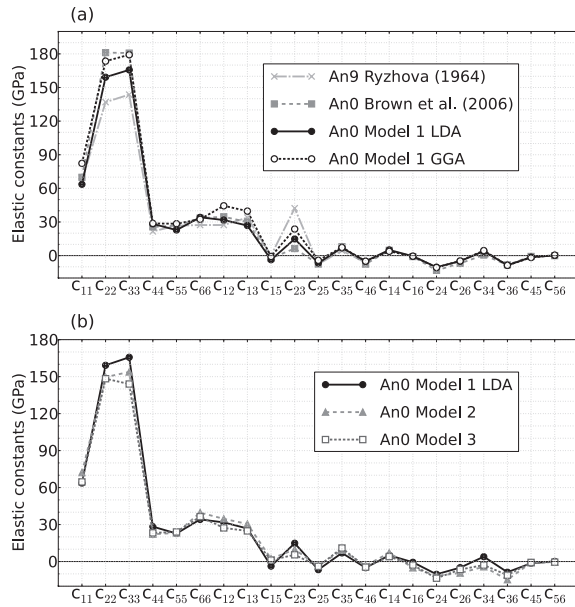


FIGURE 3. Comparison of An0 elastic constants from Table 1. (a) Our Model 1 results calculated with LDA and GGA are plotted with elastic constants measured by Ryzhova (1964) and Brown et al. (2006). (b) Results for our three An0 models.

Elastic constants

Our calculated elastic constants and experimentally found elastic constants for similar compositions are shown in Table 1. The bulk modulus (K) and shear modulus (G) were calculated for each set of the elastic constants using the Voigt, Reuss, and Hill averages (e.g., Hill 1952; Belikov et al. 1970).

An0. Model 1 results (both LDA and GGA) agree well with experimental results (Fig. 3a). Elastic constants calculated for Model 1 using LDA and GGA are both higher than many of the measurements for An9 of Ryzhova (1964) and lower than, but closer to, the elastic constants for An0 of Brown et al. (2006) (Table 1; Fig. 3a). Seront et al. (1993) estimated the C_{ij} of Ryzhova (1964) to be low by ~10%, likely because of twins, microcracks, and pores in the sample. Brown et al. (2006) estimated their errors to be much less at around 1%. While our results are within or nearly within estimated errors for Ryzhova (1964) for all C_{ij} , they are not within the estimated errors of Brown et al. (2006). However, Brown et al. (2006) mention but do not discuss the effect of actinolite inclusions; actinolite is denser (3.11 g/cm^3), and inclusions could affect velocity measurements in different directions, especially if they are oriented. They also mention large covariances when deriving elastic constants for C_{11} , C_{22} , C_{33} , C_{12} , C_{13} , and C_{23} from velocity measurements, which may partially explain the large spread in these values among the four sets of data.

Although large discrepancies exist between LDA and Brown et al. (2006) for C_{22} and C_{33} , LDA agrees better than GGA for nearly all other C_{ij} , particularly for C_{11} , C_{12} , C_{13} , and C_{23} . A closer agreement of LDA results with experimental results is evidenced in a closer match between LDA and experiments for bulk and shear moduli (Table 1). Because LDA returned a better match

than GGA to the only full set of experimentally determined plagioclase elastic constants, all other elastic constants in this study were calculated with the LDA functional.

Elastic constants for our three An0 models, compared in Table 1 and Figure 3b, are similar. Elastic constants for all three models differ up to ~10 GPa, with the exception of C_{33} for Model 1 and Model 3, which differ by 21.7 GPa. This demonstrates that placement of Al has a significant effect on elasticity. However, the fact that disordered Models 2 and 3 differ from each other by the same amount that either differ from ordered Model 1 suggests that which specific T-sites Al occupies makes little difference, only that it is distributed among different T-site types. The similarity in C_{ij} among the disordered models and ordered model is consistent with experimental observations made by Curetti et al. (2011) who discovered that disordered albite behaves similarly to ordered albite up to 4 GPa, but has a slightly lower bulk modulus. The Hill-averaged bulk modulus of Model 2 (55.3 GPa) is about the same as that of Model 1 (54.9 GPa), but Model 3 has a lower bulk modulus (49.5 GPa). At higher pressures Curetti et al. (2011) observed less shearing of tetrahedral rings in disordered albite, causing the a -axis to be stiffer and the b -axis and c -axis to be softer in disordered albite. We do not observe a softer C_{11} (corresponding to the a -axis) for disordered Model 3 compared to ordered model Model 1, but we do for Model 2. In addition, the C_{22} and C_{33} for both Model 2 and Model 3 are notably lower than for Model 1.

An50. Our calculated elastic constants for An50 are comparable to those of both Alexandrov and Ryzhova (1962) and Ryzhova (1964) (Table 1; Fig. 4a). Error estimates of Seront et al. (1993) of ~10% for Ryzhova (1964) apply here as well. As seen with the data sets for An0, the elastic constants that vary

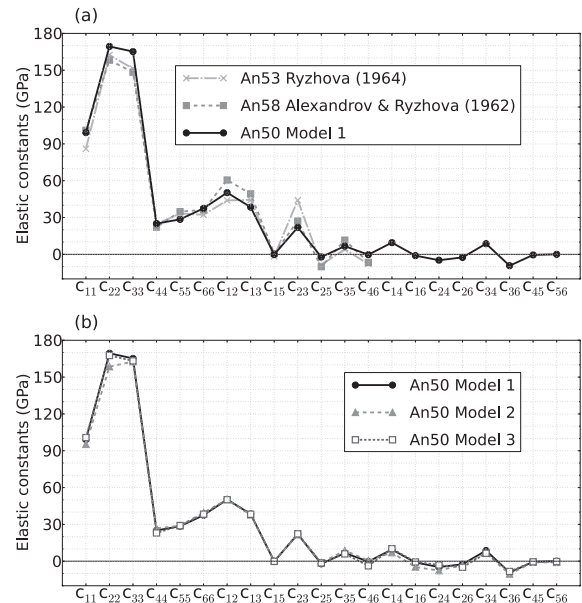


FIGURE 4. Comparison of An50 constants from Table 1. (a) Our Model 1 results are plotted with experimental results from Ryzhova (1964) and Alexandrov and Ryzhova (1962). (b) Our calculated An50 models plotted together. An50 Model 3 overlaps An50 Model 1 for most C_{ij} .

the most among data sets for An50 are C_{11} , C_{22} , C_{33} , C_{12} , C_{13} , and C_{23} . Differences in C_{22} and C_{33} among our Model 1 elastic constants and the elastic constants of Alexandrov and Ryzhova (1962) and Ryzhova (1964) are roughly 15 GPa corresponding to $\sim 10\%$, so within the approximated 10% error. However, our calculated C_{23} for Model 1 is 22.1 GPa (or $\sim 50\%$) lower than the measurements of Ryzhova (1964) and 5.1 GPa ($\sim 20\%$) lower than the measurements of Alexandrov and Ryzhova (1962). Variations may be due to compositional differences and exsolution of andesine and laboradorite (Laves et al. 1965) in Alexandrov and Ryzhova's (1962) and Ryzhova's (1964) samples.

Elastic constants for our three An50 models are compared in Table 1 and Figure 4b. Model 1 and Model 2 differ only in Al location, and elastic constants for these models agree to within 5 GPa or less for all elastic constants, except for C_{22} which is about 11 GPa higher in Model 1. These results suggest, as did comparison of our three sets of An0 results, that Al distribution alone can change elastic constants in plagioclase feldspars up to about 10 GPa. On the other hand, differences between C_{ij} are negligible for Model 1 and Model 3, which vary only in placement of Na and Ca in M-sites. While the arrangement of large cations did not affect elastic constants in this case, the ratio of large cations, Na:Ca, does seem to have a substantial effect, which we discuss below.

An100. Figure 5 compares our calculated elastic constants for An0 Model 1, An50 Model 1, and An100 and shows that stiffness increases with An-content (see also Table 1). An100's higher elastic constants may be due to the increasing number of larger Ca cations and stronger, shorter Ca-O bonds (Kroll 1983; Hackwell and Angel 1992). For all three compositions, C_{11} is the lowest of the compressional diagonal components. A much softer C_{11} is consistent with findings that hydrostatic compression of An0 is accommodated mostly by compaction of tetrahedral crankshafts in the direction perpendicular to $\{100\}$ (Angel 1994, 2004; Downs et al. 1994; Benusa et al. 2005). Our results show that as An-content increases, C_{11} greatly increases, C_{22} slightly increases, and C_{33} does not noticeably increase. This trend agrees with anisotropy studies of feldspars done by Angel et al. (2012) who discovered that much of the expansion and compression in feldspars due to compositional changes are accommodated by two tilting mechanisms of the rings of four corner-linked tetrahedra that produce a large change in distance between (100) planes, a smaller change along b , and not much change in c . The

large spread in C_{12} , C_{13} , and C_{23} among our three compositions is likely directly related to their corresponding C_{11} and these two tilting mechanisms, as suggested by compression experiments. Benusa et al. (2005) showed that compaction perpendicular to $\{100\}$ is accommodated by rotation of the tetrahedra, which in turn causes the tetrahedral rings running parallel to $[010]$ (rings shown in Fig. 2) to shear, leading to softening of C_{12} , C_{13} , and C_{23} . Conversely, compression along y and z is not accommodated by rotation of tetrahedra and shearing of tetrahedral rings, so C_{22} and C_{33} are higher.

Comparison of results among our different models for An0, An50, and An100 suggests that elastic constants are minimally affected by large cation positions within the M-sites, somewhat affected by Al positions within the T-sites, and largely affected by increasing An content, i.e., increasing the ratios Al:Si and Ca:Na. Yet these effects are not separate from each other. Increasing An content requires more T-sites to be filled with Al, and thus more T-O-T bond angles to be Al-O-Si angles and T-O bonds to be Al-O bonds. Much of the compressional behavior of plagioclase is attributed to the tilting and compression of its tetrahedral rings, which is determined by T-O-T bond angles and T-O bond lengths. While this is largely determined by Al distribution, secondary effects of M-O bonds also play a role (Angel et al. 2012). Downs et al. (1994) found Si-O-Al angles to be more compressible than Si-O-Si angles in low albite and suggested that anorthite's lower compressibility is due to the stronger Ca-O₆ bonds stiffening the Si-O-Al angles compared with the longer, weaker Na-O₆ bonds.

Velocity maps

Elastic properties may be used to calculate wave velocities in different directions through a single crystal or combined with the orientation distribution of a polycrystal to model seismic anisotropy for an aggregate with preferred orientation. Here we use the program Beartex (Wenk et al. 1998) to calculate P -wave and S -wave velocities for single crystals using elastic constants and densities (Table 1) for our An0 Model 1, An50 Model 1, and An100 structures, and for experimental results. Velocities are plotted on equal area projections in Figure 6.

Comparison of velocity maps in Figure 6a show seismic anisotropy decreases with increasing Al disorder and increasing An content for our calculated elastic constants. Experimental measurements of C_{ij} do not observe this trend (Fig. 6b), but compression experiments do. From compression experiments on analbite, Curetti et al. (2011) found ordered low albite to be more anisotropic than disordered high albite, and in compression studies of single crystals in a diamond-anvil cell, Angel et al. (1988) found An0 to be more anisotropic than An100. This is attributed to the redistribution of the more compressible Al-O-Si bonds and corresponding T-O bond lengths associated with disorder (Downs et al. 1994; Curetti et al. 2011).

In addition, we find the wave velocities become less symmetrical about $[001]$ with increasing Al-disorder and increasing An-content (Fig. 6a). Specifically, we see the fastest P -wave direction shift from $[001]$ in ordered An0 Model 1 to $\sim 5^\circ$ from the $[001]$ direction in disordered Model 3 (Fig. 6a). Correspondingly, Curetti et al. (2011) observed a rotation of the strain ellipsoid, i.e., a rotation of the directions of maximum and minimum stresses (Musgrave 1970, p. 16), when comparing ordered low albite to

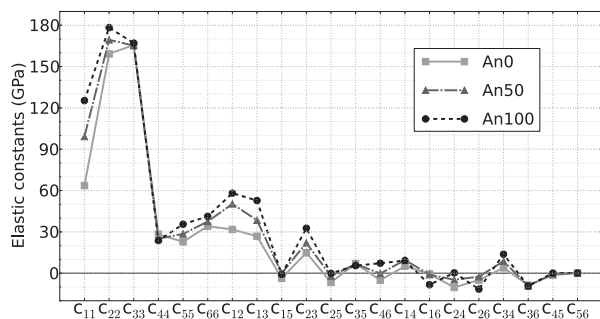


FIGURE 5. Comparison of computed An0 Model 1, An50 Model 1, and An100 elastic constants from Table 1.

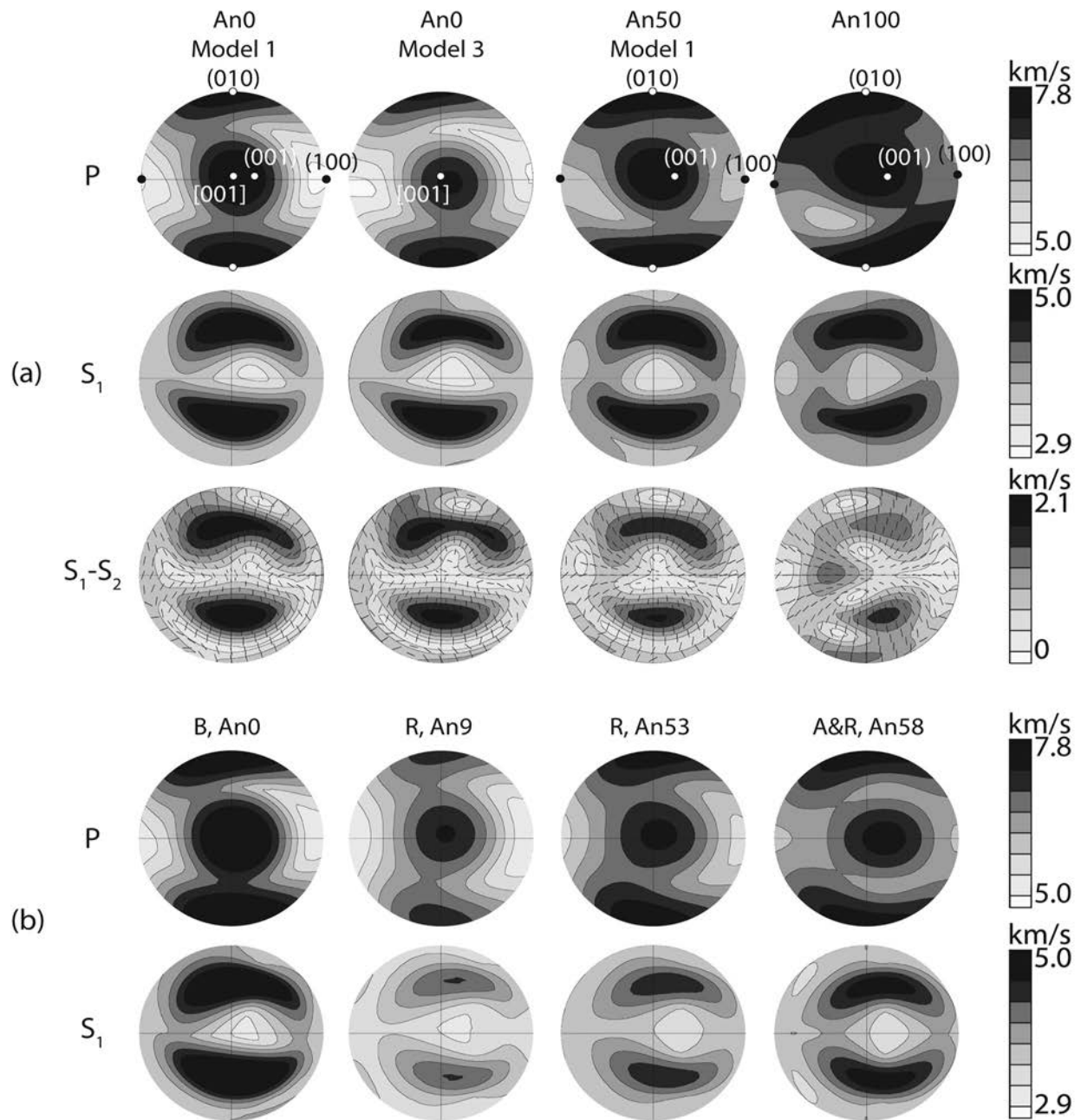


FIGURE 6. Velocity surface maps for single crystals calculated from densities and elastic constants. (a) *P*-wave, fastest *S*-wave (S_1), and shear wave splitting (S_1-S_2) overlain with S_1 -wave polarization maps (indicated with black lines) for An0 Model 1, An0 Model 3, An50 Model 1, and An100; (b) *P*-wave and fastest *S*-wave (S_1) maps calculated from the elastic constants measured for An0 by Brown et al. (2006) (B); for An9 and An53 by Ryzhova (1964) (R); and for An58 by Alexandrov and Ryzhova (1962) (A&R). Major crystallographic poles and directions have been plotted in *P*-wave velocity maps in a. Velocities are shown in grayscale in km/s (scale bars on far right). Equal area projections.

disordered high albite, suggesting that the redistribution of Al and Al-O-Si bonds is responsible for the decrease in elastic symmetry. Similarly, the slowest *P*-wave direction shifts from (100) in An0 to 55° from the (100) pole in An100 (Fig. 6a), consistent with findings of Angel et al. (1988). The redistribution of Al atoms and bonds can also help explain this rotation with increasing An content, but it may not account for the much larger shift of 55°

suggesting that either the increased amount of Al and/or Ca and associated bonds are responsible.

When shear waves enter an anisotropic medium, they split into two orthogonally polarized waves with one wave traveling slightly faster than the other. The difference between the fastest shear wave velocity (S_1) and the slowest shear wave velocity (S_2) is another measure of the extent of anisotropy. The decrease in

TABLE 2. Maximum and minimum P -wave and S -wave velocities (in km/s) and elastic anisotropy indices (A) for calculated and experimentally derived sets of elastic constants

	An0 1 LDA	An0 1 GGA	An0 2 LDA	An0 3 LDA	An0 B exp.	An9 R exp.	An50 1 LDA	An50 2 LDA	An50 3 LDA	An53 R exp.	An58 A&R exp.	An100 LDA
Max v_s	5.37	5.46	5.24	5.24	5.8	4.42	5.26	5.16	5.18	4.66	4.96	5.07
Min v_s	2.79	3.27	2.93	2.94	2.59	2.55	2.93	3.23	3.26	2.69	2.7	2.63
Max v_p	7.98	8.30	7.72	7.63	8.38	7.45	7.92	7.84	7.93	7.79	7.68	8.08
Min v_p	4.86	5.60	5.08	4.91	5.14	5.05	5.73	5.82	6.00	5.65	6.14	5.83
A	0.49	0.39	0.41	0.43	0.48	0.38	0.32	0.30	0.28	0.32	0.22	0.32

anisotropy in plagioclase with increasing An-content can also be seen by comparing S_1 - S_2 plots for An0, An50, and An100 in the third row of Figure 6a with S_1 -wave polarization directions superimposed. Polarization of S_1 -waves is similar among the three compositions. Velocity differences between S_1 and S_2 waves are 0.04–2.22 km/s for An0 Model 1, 0.01–1.87 km/s for An50 Model 1, and 0.04–1.65 km/s for An100 as compared to 0.02–0.89 for olivine, 0–1.86 km/s for quartz, 0.02–1.87 km/s for hornblende, 0.09–1.69 km/s for gypsum, 0–3.64 km/s for biotite, and 0.3–2.44 for muscovite.

An elastic anisotropy index,

$$A = 2 \times \frac{v_{P_{\max}} - v_{P_{\min}}}{v_{P_{\max}} + v_{P_{\min}}}$$

where $v_{P_{\max}}$ and $v_{P_{\min}}$ are the maximum and minimum P -wave velocities, respectively, was calculated for all sets of C_{ij} s (Table 1). The elastic anisotropy indices (A) for our three An0 models (Model 1 = 0.49, Model 2 = 0.41, Model 3 = 0.43) show that Al disorder decreases anisotropy. Anisotropy also decreases for disorder in An50 (Model 1 = 0.32, Model 2 = 0.30), but to a lesser extent. Comparison among the three compositions (An0 = 0.49, An50 = 0.32, An100 = 0.32) shows that anisotropy greatly decreases with An content until intermediate composition. This decrease is much larger than the decrease in anisotropy found by redistributing Al in the An0 structures, suggesting that Al disorder partially contributes to decreasing anisotropy, and substitution of Al for Si and Ca for Na may have equally as large of an effect. Anisotropy indices for our elastic constants are equal or higher than those calculated from the elastic constants of Brown et al. (2006) (An0 = 0.48), Ryzhova (1964) (An9 = 0.38, An53 = 0.32), and Alexandrov and Ryzhova (1962) (An58 = 0.22). Compared to the A for other common crustal minerals, e.g., olivine = 0.22, quartz = 0.28, hornblende = 0.33, gypsum = 0.36, biotite = 0.64, muscovite = 0.55, plagioclase is very anisotropic, and thus any preferred alignment of plagioclase crystals will contribute to seismic anisotropy in the crust.

IMPLICATIONS

Our elastic constants for plagioclase feldspars albite (An0), andesine/laboradorite (An50), and anorthite (An100) agree well with earlier experiments and provide a full range of plagioclase compositions from which any member of the plagioclase family can be estimated. These elastic constants can be applied to model anisotropy of plagioclase-containing rocks and are particularly useful to improving velocity calculations through the lower crust, which is largely composed of this highly anisotropic mineral. However, many seismic studies of the crust do not consider

anisotropy, which has been shown to depend much more on mineral texture than layering (Weiss et al. 1999). Previous studies of natural samples find plagioclase-rich rock to have moderately strong texture (e.g., Liebermann and Ringwood 1976; Wenk et al. 1986; Ji and Mainprice 1988; Siegesmund et al. 1989; Siegesmund and Kruhl 1991; Seront et al. 1993; Xie et al. 2003; Feinberg et al. 2006; Barreiro et al. 2007). Our calculations find plagioclase to be more elastically anisotropic than previous measurements, indicating that seismic anisotropy in the lower crust related to plagioclase texture may be greater than previously thought.

We find that elastic anisotropy decreases with An-content as the tetrahedral framework adjusts to accommodate replacement of Si with Al in T-sites and Na with Ca. In contrast to compression experiments which suggest that elastic anisotropy largely depends on Al-Si disorder, our calculations show that the difference in ratios Al:Si and Ca:Na may have an equally significant effect.

ACKNOWLEDGMENTS

P. Kaercher is grateful to Siegfried Matthies for providing the Fortran code used to rotate elastic constants into the standard convention and to Roman Vasin for help translating and understanding publications written in Russian. We also thank the Carnegie/Department of Energy Alliance Center (CDAC), the National Science Foundation (EAR 1343908) for financial support and DOE-BES (DE-FG02-05ER15637). We are appreciative to comments from editor B.B. Karki and two reviewers that helped us improve the manuscript.

REFERENCES CITED

- Abramson, E.H., Brown, J.M., and Slutsky, L.J. (1999) Applications of impulsive stimulated scattering in the earth and planetary sciences. *Annual Review of Physical Chemistry*, 50, 279–313.
- Alexandrov, K.S., and Ryzhova, T.V. (1962) Elastic properties of rock-forming minerals: III feldspars. *Bulletin of the Academy of Sciences, USSR, Geophysical Series*, 10, 129–131.
- Alexandrov, K.S., Alchikov, U.V., Belikov, B.P., Zalavskii, B.I., and Krupnyi, A.I. (1974) Velocities of elastic waves in minerals at atmospheric pressure and increasing precision of elastic constants by means of EVM. *Bulletin of the Academy of Sciences, USSR, Geological Survey*, 10, 15–24.
- Angel, R.J. (1994) Feldspars at high pressure. In I. Parsons, Ed., *Feldspars and their Reactions, Series C: Mathematical and Physical Sciences*, 421, p. 271–312. Kluwer, Dordrecht.
- (2004) Equations of state of plagioclase feldspars. *Contributions to Mineralogy and Petrology*, 146, 506–512.
- Angel, R.J., Hazen, R.M., McCormick, T.C., Prewitt, C.T., and Smyth, J.R. (1988) Comparative compressibility of end-member feldspars. *Physics and Chemistry of Minerals*, 15, 313–318.
- Angel, R.J., Sochalski-Kolbus, L.M., and Tribadino, M. (2012) Tilts and tetrahedral: the origin of the anisotropy of feldspars. *American Mineralogist*, 97, 765–778.
- Bambauer, H.U., Eberhard, E., and Viswanathan, K. (1967) The lattice constants and related parameters of “plagioclases (low).” Part IV of laboratory investigations on plagioclases. *Structural Materials Property Manual*, 47, 351–364.
- Barreiro, J.G., Lonardelli, I., Wenk, H.R., Dresen, G., Rybacki, E., Ren, Y., and Tomé, C.N. (2007) Preferred orientation of anorthite deformed experimentally in Newtonian creep. *Earth and Planetary Science Letters*, 264, 188–207.
- Bass, J.D. (1995) Elasticity of minerals, glasses, and melts. In T.J. Ahrens, Ed., *Mineral Physics and Crystallography: A handbook of physical constants. American Geophysical Union reference shelf*, 2, 45–63 p. Washington, D.C.
- Belikov, B.P., Aleksandrov, K.S., and Ryzhova, T.V. (1970) Elastic Properties of

- Rock-Forming Minerals and Rocks, p. 276. Nauka, Moscow (in Russian).
- Benna, P., Zanini, G., and Bruno, E. (1985) Cell parameters of thermally treated anorthite Al, Si configurations in the average structures of the high temperature calcic plagioclases. *Contributions to Mineralogy and Petrology*, 90, 381–385.
- Benusa, M.D., Angel, R.J., and Ross, N.L. (2005) Compression of albite, $\text{NaAlSi}_3\text{O}_8$. *American Mineralogist*, 90, 1115–1120.
- Brown, J.M., Abramson, E.H., and Angel, R.J. (2006) Triclinic elastic constants for low albite. *Physics and Chemistry of Minerals*, 33, 256–265.
- Carpenter, M.A., McConnell, J.D.C., and Navrotsky, A. (1985) Enthalpies of ordering in the plagioclase feldspar solid solution. *Geochimica et Cosmochimica Acta*, 49, 947–966.
- Carpenter, M.A., Angle, R.J., and Finger, L.W. (1990) Calibration of Al/Si order variations in anorthite. *Contributions to Mineralogy and Petrology*, 104, 471–480.
- Ceperley, D.M., and Alder, B.J. (1980) Ground state of the electron gas by a stochastic method. *Physical Review Letters*, 45, 566–569.
- Curetti, N., Sochalski-Kolbus, L.M., Angel, R.J., Benna, P., Nestola, F., and Bruno, E. (2011) High-pressure structural evolution and equation of state of analbite. *American Mineralogist*, 96, 383–392.
- Downs, R.T., Hazen, R.M., and Finger, L.W. (1994) The high-pressure crystal chemistry of low albite and the origin of the pressure dependency of Al-Si ordering. *American Mineralogist*, 79, 1042–1052.
- Every, A.G., and McCurdy, A.K. (1992) Numerical data and functional relationships in science and technology. In O. Madelung, Ed., *Landoldt-Börnstein*, new series, group III, 29a. Springer-Verlag, Berlin.
- Feinberg, J., Wenk, H.R., Scott, G.R., and Renne, P.R. (2006) Preferred orientation and anisotropy of seismic and magnetic properties in gabbro-norites from the Bushveld layered intrusion. *Tectonophysics*, 420, 345–356.
- Ferguson, R.B., Traill, R.J., and Taylor, W.H. (1958) The crystal structures of low-temperature and high-temperature albites. *Acta Crystallographica*, 11, 331–348.
- FitzGerald, J.D., Parise, J.B., and Mackinnon, I.D.R. (1986) Average structure of an An_{48} plagioclase from the Hogarth Ranges. *American Mineralogist*, 71, 1399–1408.
- Hacker, B.R., and Abers, G.A. (2004) Subduction factory 3: An Excel worksheet and macro for calculating the densities, seismic wave speeds, and H_2O contents of minerals and rocks at pressure and temperature. *Geochemistry Geophysics Geosystems*, 5, Q01005, <http://dx.doi.org/10.1029/2003GC000614>.
- Hackwell, T.P., and Angel, R.J. (1992) The comparative compressibility of reedmergnerite, danburite and their aluminium analogs. *European Journal of Mineralogy*, 4, 1221–1227.
- Harlow, G.E., and Brown, G.E. (1980) Low albite: an X-ray and neutron diffraction study. *American Mineralogist*, 65, 986–995.
- Hill, R. (1952) The elastic behaviour of crystalline aggregate. *Proceedings of the Physical Society A*, 65, 349–354.
- Hohenberg, P., and Kohn, W. (1965) Inhomogeneous electron gas. *Physical Review*, 136, 3B, 864–871.
- Ji, S., and Mainprice, D. (1988) Natural deformation fabrics of plagioclase: Implications for slip systems and seismic anisotropy. *Tectonophysics*, 147, 145–163.
- Karki, B.B., Warren, M.C., Stixrude, L., Ackland, G.J., and Crain, J. (1997) Ab initio studies of high-pressure structural transformations in silica. *Physical Review B*, 55, 3465.
- Kempster, C.J.E., Megaw, H.D., and Radoslovich, E.W. (1962) The structure of anorthite, $\text{CaAl}_2\text{Si}_2\text{O}_8$. I. Structure analysis. *Acta Crystallographica*, 15, 1005–1017.
- Kohn, W., and Sham, L.J. (1964) Self-consistent equations including exchange and correlation effects. *Physical Review*, 140, 4A, 1133–1138.
- Kresse, G., and Furthmüller, J. (1996) Efficient iterative schemes for *ab initio* total-energy calculations using a planewave basis set. *Physical Review B*, 54, 11169–11186.
- Kresse, G., and Hafner, J. (1993) Ab initio molecular dynamics for liquid metals. *Physical Review B*, 47, 558–561.
- Kroll, H. (1983) Lattice parameters and determinative methods for plagioclase and ternary feldspars. In P.H. Ribbe, Ed., *Feldspar Mineralogy*. Reviews in Mineralogy and Geochemistry, 2nd ed., 2, 101–119.
- Kroll, H., and Müller, W.F. (1980) X-ray and electron-optical investigation of synthetic high-temperature plagioclases. *Physics and Chemistry of Minerals*, 5, 255–277.
- Kunz, M., and Armbruster, T. (1990) Difference displacement parameters in alkali feldspars: Effects of (Si,Al) order-disorder. *American Mineralogist*, 75, 141–149.
- Laves, F., and Chassignon, U. (1950) An X-ray investigation of the “high”-“low” albite relations. *The Journal of Geology*, 58, 584–592.
- Laves, F., Nissen, H.U., and Bollmann, W. (1965) On schiller and submicroscopic lamellae of labradorite (Na,Ca)(Si,Al)₃O₈. *Naturwissenschaften*, 52, 427–428.
- Liebermann, R.C., and Ringwood, A.E. (1976) Elastic properties of anorthite and the nature of the lunar crust. *Earth and Planetary Science Letters*, 31, 69–74.
- Loewenstein, W. (1954) The distribution of aluminium in the tetrahedral of silicates and aluminates. *American Mineralogist*, 39, 92–96.
- Megaw, H.D. (1956) Notation for feldspar structures. *Acta Crystallographica*, 9, 56.
- Megaw, H.D., Kempster, C.J.E., and Radoslovich, E.W. (1962) The structure of anorthite, $\text{CaAl}_2\text{Si}_2\text{O}_8$. II. Description and discussion. *Acta Crystallographica*, 15, 1017–1035.
- Miltzer, B., Wenk, H.R., Stackhouse, S., and Stixrude, L. (2011) First-principles calculation of the elastic moduli of sheet silicates and their application to shale anisotropy. *American Mineralogist*, 96, 125–137.
- Monkhorst, H.J., and Pack, J.D. (1976) Special points for Brillouin-zone integrations. *Physical Review B*, 13, 5188–5192.
- Musgrave, M.J.P. (1970) *Crystal Acoustics: Introduction to the study of elastic waves and vibrations in crystals*. Holden-Day, San Francisco, California.
- Nye, J.F. (1984) *Physical Properties of Crystals*. Clarendon Press, Oxford.
- Perdew, J.P., Burke, K., and Ernzerhof, M. (1996) Generalized gradient approximation made simple. *Physical Review Letters*, 77, 3865–3868.
- Prewitt, C.T., Sueno, S., and Papike, J.J. (1976) The crystal structures of high albite and monalbite at high temperatures. *American Mineralogist*, 61, 1213–1225.
- Ribbe, P.H. (1983) Chemistry, structure and nomenclature of feldspars. In P.H. Ribbe, Ed., *Feldspar Mineralogy*. Reviews in Mineralogy and Geochemistry, 2nd ed., 2, 1–19.
- Ribbe, P.H., Megaw, H.D., and Taylor, W.H. (1969) The albite structures. *Acta Crystallographica*, B, 25, 1503–1518.
- Ryzhova, T.V. (1964) Elastic properties of plagioclase. *Bulletin of the Academy of Sciences, USSR, Geophysical Series*, 7, 633–635.
- Seront, B., Mainprice, D., and Christensen, N.I. (1993) A determination of the three-dimensional seismic properties of anorthosite: Comparison between values calculated from the petrofabric and direct laboratory measurements. *Journal of Geological Research*, 98, 2209–2221.
- Siegesmund, S., and Kruhl, J.H. (1991) The effect of plagioclase textures on velocity anisotropy and shear wave splitting at deeper crustal levels. *Tectonophysics*, 191, 147–154.
- Siegesmund, S., Takeshita, T., and Kern, H. (1989) Anisotropy of V_p and V_s in amphibolites of the deeper crust and its relationship to the mineralogical, microstructural and textural characteristics of the rock. *Tectonophysics*, 157, 25–38.
- Simmons, G., and Wang, H. (1971) *Single crystal elastic constants and calculated aggregate properties: A handbook*, 2nd ed., 370 p. MIT Press, Cambridge.
- Smith, J.V., and Brown, W.L. (1988) *Feldspar Minerals: Crystal structures, Physical, chemical, and microtextural properties*, 2nd ed., 1. Springer-Verlag, Berlin.
- Sochalski-Kolbus, L.M., Angel, R.J., and Nestola, F. (2010) The effect of Al/Si disorder on the bulk moduli of plagioclase feldspars. *Mineralogical Magazine*, 74, 943–950.
- Standards on Piezoelectric Crystals (1949) *Proceedings of the IRE*, vol.37, no.12, pp. 1378,1395, Dec. 1949, <http://dx.doi.org/10.1109/JRPROC.1949.229975>.
- Stewart, D.B., and Ribbe, P.H. (1969) Structural explanation for variations in cell parameters of alkali feldspars with Al/Si ordering. *American Journal of Science*, Schairer 267-A, 444–462.
- Tribaudo, M., and Angel, R. (2012) The thermodynamics of the *J1-P1* phase transition in Ca-rich plagioclase from an assessment of the spontaneous strain. *Physics and Chemistry of Minerals*, 39, 699–712.
- Tuttle, O.F., and Bowen, N.L. (1950) High-temperature albite and contiguous feldspars. *The Journal of Geology*, 58, 572–583.
- Wainwright, J.E., and Starkey, J. (1971) A refinement of the structure of anorthite. *Zeitschrift für Kristallographie*, 133, 75–84.
- Waldbaum, D.R., and Robie, R.A. (1971) Calorimetric investigation of Na-K mixing and polymorphism in the alkali feldspars. *Journal of Crystallography*, 134, 381–420.
- Weiss, T., Siegesmund, S., Rabbel, W., Bohlen, T., and Pohl, M. (1999) Seismic velocities and anisotropy of the lower continental crust: A review. *Pure and Applied Geophysics*, 156, 97–122.
- Wenk, H.R., and Kroll, H. (1984) Analysis of $P\bar{1}$, $\bar{1}1$ and $C\bar{1}$ plagioclase structures. *Bulletin de Mineralogie, Petrologie et Geochemie*, 107, 467–487.
- Wenk, H.R., Bunge, H.J., Jansen, E., and Pannetier, J. (1986) Preferred orientation of plagioclase—neutron diffraction and U-stage data. *Tectonophysics*, 126, 271–284.
- Wenk, H.R., Matthies, S., Donovan, J., and Chateigner, D. (1998) BEARTEX: A Windows-based program system for quantitative texture analysis. *Journal of Applied Crystallography*, 31, 262–269.
- White, C.E., Provis, J.L., Riley, D.P., Kearley, G.J., and van Deventer, J.S.J. (2009) What is the structure of kaolinite? Reconciling theory and experiment. *Journal of Physics and Chemistry B*, 113, 6756–6765.
- Winter, J.K., Okamura, F.P., and Ghose, S. (1979) A high-temperature structural study of high albite, monalbite, and the analbite → monalbite phase transition. *American Mineralogist*, 64, 409–423.
- Xie, Y., Wenk, H.R., and Matthies, S. (2003) Plagioclase preferred orientation by TOF neutron diffraction and SEM-EBSD. *Tectonophysics*, 370, 269–286.